Modeling of a quantum dot gain chip in an external cavity laser configuration

Jannik F Ehlert[1,2,*] ![ORCID]**, Alain Mugnier**[1]**, Gang He**[3] **and Frédéric Grillot**[2,4] ![ORCID]

[1] EXFO Optics, 4 rue Louis de Broglie, 22300 Lannion, France
[2] LTCI, Télécom Paris, Institut Polytechnique de Paris, 91120 Palaiseau, France
[3] EXFO Inc., Québec (Québec) G1M 2K2, Canada
[4] Center for High Technology Materials, University of New-Mexico, Albuquerque, NM 87106, United States of America

E-mail: jannik.ehlert@telecom-paris.fr

Abstract

External cavity semiconductor lasers with strong optical feedback already exist using a gain chip medium. Owing to their ultrafast carrier dynamics, strong output power, and high temperature reliability, quantum dots as a gain medium are now envisioned as a promising solution to replace the current quantum well technology. This paper presents a semi-analytical rate equation model which is used to describe a quantum dot gain chip capable of lasing only with a free space external cavity laser. It investigates the evolution of the dynamical properties such as the turn-on delay and the damping rate. It also confirms the model's validity through the relative intensity noise and the frequency noise with respect to both material and device parameters like the linewidth enhancement factor, the gain compression factor, or the cavity length. Overall, this numerical investigation provides initial building blocks for future fabrication research and development of high performance devices including filters or gratings as wavelength-selective components.

Keywords: external cavity, semiconductor laser, quantum dots, optical feedback, Langevin noise

(Some figures may appear in color only in the online journal)

1. Introduction

Tunable external cavity (EC) diode lasers are known to be of considerable interest for a wide range of applications including but not limited to coherent optical telecommunications, atomic and molecular laser spectroscopy, precise measurements, and environmental monitors [1, 2]. With the tremendous efforts dedicated to the improvement of semiconductor lasers using high-quality materials and optimization of the device structure, tunable EC diode lasers have become of paramount importance for the aforementioned applications. The simplest way of achieving tunability is by using a semiconductor diode laser with or without antireflection (AR) facet coatings combined with a collimator for coupling the laser's output and an external mode-selection filter [2]. For instance,

diffraction gratings built in a Littman-Metcalf and Littrow cavity configuration can be used to provide selective optical feedback for single-mode operation. Thus, by rotation of the mirror or the diffraction grating depending on the configuration [3], wavelength tunability is achieved over the entire gain bandwidth in single-mode operation. However, it is known that depending on the EC configuration and the laser diode parameters, the desired performance can be substantially affected. In order to further control the tunability, the nature of the gain media is of vital importance.

Although quantum well (QW) technology is already commercially used in any EC semiconductor laser, the use of quantum dot (QD) nanostructures as active media have demonstrated multiple advantages for the realization of high performance devices. In particular, with an inhomogeneous broadening as an intrinsic behavior of nanostructures containing QDs, the amplified spontaneous emission of the gain

---

medium contributes to the desired wide band tunability. The wider the wavelength spectrum, the wider the external cavity laser's potential tunability. Together with a higher temperature stability [4] and a lower threshold current for a QD laser compared to its QW counterparts [5, 6], lasing appears to be more likely over the full range including different temperature variations [7].

In this work, the final goal is to have a much wider tuning range than what is possible or available today with QW external cavity lasers, i.e. 140 nm around the telecom O-band or 200 nm around the telecom C-band. Besides, a smaller linewidth enhancement factor in QD lasers contributes to a lower phase noise [8] hence transforming into a natural spectral linewidth not exceeding a few hundreds of kilohertz [9]. The spectral line can be further reduced by using a proper EC [10]. Additionally, when an external cavity laser is combined with the filtering properties of a diffraction grating, a very good signal to noise ratio can be achieved. Making an already low intensity noise possible with a QW gain chip, one expects much better properties from the QD gain chip due to the large damping factor, which further reduces the intensity noise. Last but not least, it has also been shown that QD lasers have a great potential for large-scale and low-cost photonics integration by overcoming inherent problems related to standard diode lasers integrated on silicon [11–13]. All these properties suggest that similar improved performance can be expected with EC QD lasers in combination with high operating temperature stability, large output power, reduced noise properties, and wide tunability [1, 14].

When a semiconductor laser diode is placed in an EC, five optical feedback regimes are generally observed. According to this feedback classification [15], when the external optical feedback strength does not exceed 1%, the laser operates within the first four regimes. Thus, depending on the feedback conditions, the diode laser can either be found stable with a strong dependence on the feedback phase hence leading for instance to a narrower spectral linewidth [16] or independent but with strong chaotic pulsations such as within the coherence collapse whereby the laser optical power behaves in an erratic manner [17]. The study of these regimes are obviosuly out of the scope of the present work since they do not correspond to what is required for wavelength selection and wide tuning operation. Instead, when considering an optical feedback strength typically of several percent, the laser can transition towards regime five that is to say the so-called EC regime. In this configuration, several round trips of traveling light occur within the EC. However, if not great care is taken on the laser design, unwanted optical feedback can still exist and triggers a coherence collapse operation [15, 16].

To overcome this issue of coherence collapse, a semiconductor optical amplifier (SOA) with tilted facets is usually placed in a compound cavity, describing a regime that is not further classified: with this gain chip, mode solutions are predicted to be perfectly stable with narrow linewidths, independent of the feedback phase and any additional perturbations owing to the specific angled waveguide design with almost no

loss in propagation across the semiconductor-air interface and the complete free-space EC [16, 18].

In this paper, one focuses on the study of a QD gain chip based laser. The gain chip is by design incapable of lasing by itself, but as it is forming a compound cavity allowing lasing, the principal effect of our EC is exploited, so that many key laser parameters are investigated. In a prior work, a semi-analytical rate equation model of the coupled rate equations including both lasing and non-lasing states of the QDs as well as the Langevin noise sources [8] was originally proposed. Here we go a step forward by conducting a comprehensive analysis and providing a numerical analysis of the dynamical properties of the QD gain chip based EC laser such as the turn-on delay, the damping rate, the relative intensity noise, and the frequency noise with respect to both material and device parameters. More particularly, the impact of the linewidth enhancement factor, gain nonlinearities, and facet coating impairment is deeply investigated. Last but not least, simulations also shed the light on the importance of the EC length, as the photon lifetime gets significantly longer through a loss-free propagation in the majority of the compound cavity.

This paper is organized as follows. In section 2, the theoretical model is presented, starting from the coupled rate equations and followed by a small-signal analysis. Section 3 presents the numerical simulation results and the discussions. Finally, we summarize the main achievements in section 4. The presented numerical investigations of a QD gain chip based EC laser provide a basis for future fabrication research or developing devices with wavelength-filtering.

2. Semi-analytical model

The laser under study consists of a QD gain chip operating in free-space (figure 1). We define a laser as a device capable of lasing, which the gain chip itself is not, but the complete compound cavity consisting of the active semiconductor medium and the air-filled EC, including the low-loss interface in between. Therefore, the round trip time τ_{ext} of light in the EC determined by the length ℓ_{ext}, terminated by the external mirror (with a power reflectivity $R_3 = 0.32$). This third mirror located at $z = \ell_{\text{int}} + \ell_{\text{ext}}$ is the main output of the laser for the photons. The second light output is at the rear facet of the gain chip with a reflectivity $R_1 = 0.95$ at $z = 0$, and thus much smaller than the main output. In this work, the front facet of the gain chip has a very low power reflectivity R_2 due to an anti-reflection (AR) coating. In practice, we assume that an angled waveguide design further lowers the effective reflectivity of this front facet. The active region consists of one QD ensemble, where a wetting layer (reservoir RS) serves as the interconnection of all QDs, as seen in figure 2. Under this assumption, the numerical model includes two more energy levels: a two-fold degenerate ground state (GS) and a four-fold degenerate excited state (ES). Electrons and holes are treated as electron–hole pairs, which means that the system is in excitonic energy state, so that the QDs are assumed to be
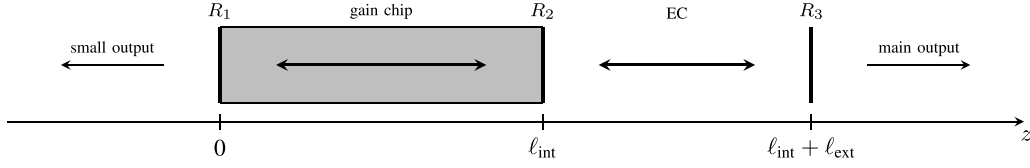
Figure 1. The external cavity (EC) laser has a length of ℓ_{ext} and a round trip time of τ_{ext} within mirror reflectivities R. The light output of the gain chip at the rear facet (reflectivity R_1 at $z = 0$) is much smaller than the main output at $z = \ell_{\text{int}} + \ell_{\text{ext}}$. In this work, the front facet mirror reflectivity R_2 is anti-reflection coated for the EC operation.
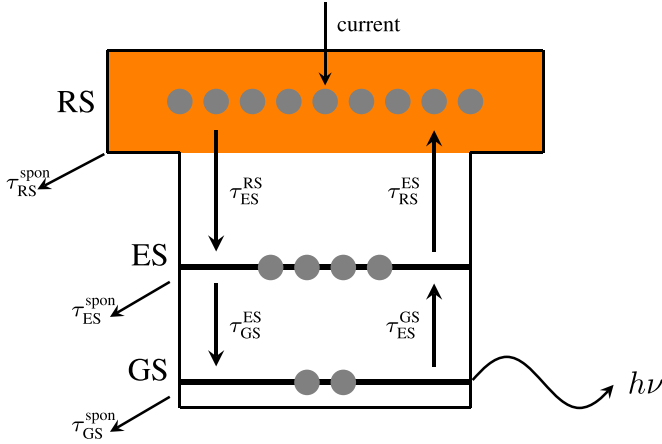

Figure 2. The electronic structure depicting the carrier dynamics including a reservoir state (RS), an excited state (ES), and a ground state (GS), transition times between the different energy levels, spontaneous emission from GS, ES and RS, as well as stimulated photons from GS [24].

always neutral. Carrier injection happens directly via RS level contacts. As a result, the carrier dynamics in the barrier are not taken into account in the model.

2.1. Rate equations

According to [8] and the schematic representation displayed in figure 2, $\tau_{\text{ES}}^{\text{RS}}$—although already described as carrier-dependent by a semi-empirical model [19]—represents the capture time from RS to ES, whereas $\tau_{\text{GS}}^{\text{ES}}$ is the relaxation time from ES to GS. On the other hand, carriers can also be thermally re-emitted from the ES to the RS level with an escape time $\tau_{\text{RS}}^{\text{ES}}$, which is governed by the Fermi distribution for the quasi-thermal equilibrium without external excitation. Similar dynamic behavior is followed by the carrier population on the GS level with regard to the ES, expressed by the escape time $\tau_{\text{ES}}^{\text{GS}}$. The contribution of the spontaneous emission is represented for each level by $\tau_{\text{RS,ES,GS}}^{\text{spon}}$. In this work, the direct capture from RS to GS [20] as well as all the contribution of the higher non-lasing states are neglected [19]. As a consequence of that, the rate equations on carriers are expressed as follows:

$$\frac{dN_{\text{RS}}}{dt} = \frac{\eta_i I}{q} + \frac{N_{\text{ES}}}{\tau_{\text{RS}}^{\text{ES}}} - \frac{N_{\text{RS}}}{\tau_{\text{ES}}^{\text{RS}}}f_{\text{ES}} - \frac{N_{\text{RS}}}{\tau_{\text{RS}}^{\text{spon}}} + F_{\text{RS}} \quad (1)$$

$$\frac{dN_{\text{ES}}}{dt} = \frac{N_{\text{RS}}}{\tau_{\text{ES}}^{\text{RS}}}f_{\text{ES}} + \frac{N_{\text{GS}}}{\tau_{\text{ES}}^{\text{GS}}}f_{\text{ES}} - \frac{N_{\text{ES}}}{\tau_{\text{RS}}^{\text{ES}}}$$
$$- \frac{N_{\text{ES}}}{\tau_{\text{GS}}^{\text{ES}}}f_{\text{GS}} - \frac{N_{\text{ES}}}{\tau_{\text{ES}}^{\text{spon}}} + F_{\text{ES}} \quad (2)$$

$$\frac{dN_{\text{GS}}}{dt} = \frac{N_{\text{ES}}}{\tau_{\text{GS}}^{\text{ES}}}f_{\text{GS}} - \frac{N_{\text{GS}}}{\tau_{\text{ES}}^{\text{GS}}}f_{\text{ES}} - \frac{N_{\text{GS}}}{\tau_{\text{GS}}^{\text{spon}}} - \Gamma_p g v_g N_p + F_{\text{GS}} \quad (3)$$

where $N_{\text{RS}}, N_{\text{ES}}$, and N_{GS} are the carrier numbers in RS, ES, and GS, respectively; q the electronic charge, Γ_p the optical confinement factor, I the bias current, η_i the injection efficiency, $F_{\text{RS,ES,GS}}$ are the Langevin noise sources for the carriers in RS, ES, and GS, respectively, v_g the group velocity,

$$f_{\text{GS}} = 1 - \frac{N_{\text{GS}}}{2N_B} \quad \text{and} \quad f_{\text{ES}} = 1 - \frac{N_{\text{ES}}}{4N_B} \quad (4)$$

the Pauli blocking factors (related to the occupation probability $\rho = f - 1$ [19]) and the GS gain defined as [21]

$$g = \frac{a(N_{\text{GS}} - N_B)}{V_{\text{QD}}(1 + \varepsilon N_p/V_p)} \quad (5)$$

where a is the differential gain associated to the GS transition, ε the nonlinear gain compression factor, V_p the confinement volume, V_{QD} the total volume of occupied by the QDs, i.e. active region volume, and N_B the total dot number. The photon number N_p and the phase ϕ equations incorporating the feedback terms are given in equations (6) and (7) [21, 22],

$$\frac{dN_p}{dt} = \left(\Gamma_p g v_g - \frac{1}{\tau_p}\right)N_p + \beta_{SP}\frac{N_{\text{GS}}}{\tau_{\text{GS}}^{\text{spon}}}$$
$$+ 2\kappa\sqrt{N_p(t)N_p(t - \tau_{\text{ext}})}\cos(\omega_0\tau_{\text{ext}} + \phi(t)$$
$$- \phi(t - \tau_{\text{ext}})) + F_{N_p} \quad (6)$$

$$\frac{d\phi}{dt} = \frac{\alpha_H}{2}\left(\Gamma_p g v_g - \frac{1}{\tau_p}\right) - \kappa\sqrt{\frac{N_p(t - \tau_{\text{ext}})}{N_p(t)}}$$
$$\times \sin(\omega_0\tau_{\text{ext}} + \phi(t) - \phi(t - \tau_{\text{ext}})) + F_\phi \quad (7)$$

where τ_{ext} is the round trip time in the free space EC of length ℓ_{ext}, α_H the linewidth enhancement factor, F_{N_p} and F_ϕ the Langevin noise sources for photons and phase, respectively,

ω_0 the angular lasing frequency without EC (solitary case), β_{SP} the spontaneous emission factor, κ the feedback strength expressed assuming $R_2 \ll 1$ as

$$\kappa = \sqrt{\frac{R_2}{R_3}} \cdot \frac{1}{\tau_{\text{ext}}} \tag{8}$$

and τ_p the mirror- and material-dependent photon lifetime based on [18, 23], following the general expression

$$1/\tau_p = v_g(\alpha_{in} + \alpha_m) \tag{9}$$

where $v_g = c/n_g$ is the material group velocity, n_g the refractive index in the active region, c the speed of light in vacuum, α_{in} the internal material losses and α_m the mirror losses. For a solitary laser, the latter are commonly expressed as

$$\alpha_m = \frac{\ln(R_a R_b)}{L} \tag{10}$$

where R are the power reflectivities of both end facets a and b and L the refractive index-dependent optical length in between the end facets.

At first sight, it might seem as if we were analyzing the properties of a laser diode under strong optical feedback. But although the feedback strength is well beyond 1% of the emitted light—which would be already a lot for a solitary semiconductor laser—one single round trip is assumed. This is possible because the complete cavity is a compound cavity which includes an AR coated gain chip front facet. Therefore, this second mirror with reflectivity R_2 reflects almost nothing back into the internal cavity additionally owing to the tilted waveguide front facet. One could also consider this second mirror as a small perturbation of a principal laser cavity which we consider as the external one here. As a result, for $R_2 \ll R_3$, or put differently: if the product of the feedback strength κ and the EC round trip time τ_{ext} is small, i.e. $\ll 1$, one round trip only needs to be taken into account [18], which is exactly what happens in the case under study.

It is important to see that R_2 is only a small perturbation in between mirror reflectivities R_1 and R_3 as explained in the paragraph above, so that the accordingly adapted mirror losses given by (10) can be put into (9), which leads to the photon lifetime being expressed as

$$\tau_p = \left(v_g \alpha_{in} + \frac{c \cdot \ln(R_1 R_3)}{2(n_g \ell_{\text{int}} + \ell_{\text{ext}})} \right)^{-1} \tag{11}$$

where R_3 is the reflectivity of mirror 3, and ℓ_{int} the internal cavity length of the gain chip, i.e. the active medium.

Turn-on dynamics and steady-state solutions of these coupled equations are numerically simulated using MATLAB© for which the used function for solving the delay differential equations is dde23 [25].

Linearizing above five rate equations (1)–(3), (6), and (7) with the small signal analysis, using Taylor polynomial

approximations, and neglecting higher order terms, results in a 5×5 matrix [21, 26]:

$$\begin{bmatrix} \gamma_{11} + j\omega & -\gamma_{12} & 0 & 0 & 0 \\ -\gamma_{21} & \gamma_{22} + j\omega & -\gamma_{23} & 0 & 0 \\ 0 & -\gamma_{32} & \gamma_{33} + j\omega & -\gamma_{34} & 0 \\ 0 & 0 & -\gamma_{43} & \gamma_{44} + j\omega & -\gamma_{45} \\ 0 & 0 & -\gamma_{53} & -\gamma_{54} & \gamma_{55} + j\omega \end{bmatrix}$$

$$\cdot \begin{bmatrix} \delta N_{\text{RS}} \\ \delta N_{\text{ES}} \\ \delta N_{\text{GS}} \\ \delta N_p \\ \delta\phi \end{bmatrix} = \frac{\delta I}{q} \begin{bmatrix} 1 \\ 0 \\ 0 \\ 0 \\ 0 \end{bmatrix} \tag{12}$$

with γ_{ij} the matrix elements as detailed by [21], ω the angular modulation frequency, and δX the modulation amplitude of parameter X.

The phase influence in the delay term of equations (6) and (7) is approximated from the steady-state conditions such that [21]

$$\cos\left(\omega_0 \tau_{\text{ext}} + \phi(t) - \phi(t - \tau_{\text{ext}})\right)$$
$$\approx P\left[1 + \alpha_H \delta\phi\left(1 - e^{-j\omega\tau_{\text{ext}}}\right)e^{j\omega t}\right] \tag{13}$$

$$\sin\left(\omega_0 \tau_{\text{ext}} + \phi(t) - \phi(t - \tau_{\text{ext}})\right)$$
$$\approx P\left[-\alpha_H + \delta\phi\left(1 - e^{-j\omega\tau_{\text{ext}}}\right)e^{j\omega t}\right] \tag{14}$$

with $P = (1 + \alpha_H^2)^{-0.5}$.

The relaxation oscillation frequency f_{R} and the damping factor γ can be obtained either from the RIN spectrum or from the calculation based on the above matrix elements [24].

2.2. Noise expressions

In what follows, two noise features are analyzed at first. Therefore, the relative intensity noise is expressed as [4, 8]

$$\text{RIN}(\omega) = \frac{|\delta N_p(\omega)|^2}{N_p^2} \tag{15}$$

and second, the frequency noise, expressed as

$$\text{FN}(\omega) = \left| \frac{\omega}{2\pi} \delta\phi(\omega) \right|^2. \tag{16}$$

Simulations include the Langevin noise sources for the carriers $F_{\text{RS,ES,GS}}$, the photons F_{N_p} and the phase F_ϕ in the form of the so-called diffusion coefficients identical to [4, 21]. Based on small signal analysis and Laplace expansion for determinants, the RIN is thus expressed as [27]

Table 1. Material and laser parameters [4, 21, 24].

Symbol	Definition	Value
a_{GS}	GS differential gain	5×10^{-15} cm^2
α_{in}	loss of internal cavity	5 cm^{-1}
β_{SP}	spontaneous emission factor	10^{-4}
Γ_p	optical confinement factor	0.06
E_{RS}	RS energy	0.97 eV
E_{ES}	ES energy	0.87 eV
E_{GS}	GS energy	0.82 eV
η_i	bias current injection efficiency	0.12
h_{QD}	QD thickness/layer height	5 nm
ℓ_{int}	active medium length	1.1 mm
W	active medium width	$3\ \mu$m
N	number of QD layers	5
n_g	refractive index (internal cavity)	3.27
τ_{ES}^{RS}	RS to ES capture time	25.1 ps
τ_{GS}^{ES}	ES to GS relaxation time	11.6 ps
τ_{RS}^{ES}	ES to RS escape time	5.8 ns
τ_{ES}^{GS}	GS to ES escape time	42.9 ps
$\tau_{RS,ES}^{spon}$	RS/ES spontaneous emission time	0.5 ns
τ_{GS}^{spon}	GS spontaneous emission time	1.2 ns

$$
\begin{aligned}
\text{RIN} = \frac{1}{N_p^2 |D|^2} &\Big[\langle |F_{RS}|^2 \rangle |D_{N_{RS}N_p}|^2 \\
&+ \langle |F_{ES}|^2 \rangle |D_{N_{ES}N_p}|^2 + \langle |F_{GS}|^2 \rangle |D_{N_{GS}N_p}|^2 \\
&+ \langle |F_{N_p}|^2 \rangle |D_{N_p N_p}|^2 + \langle |F_\phi|^2 \rangle |D_{\phi N_p}|^2 \\
&- 2 \langle F_{RS}F_{ES} \rangle \text{Re}(D_{N_{RS}N_p}D_{N_{ES}N_p}^*) \\
&- 2 \langle F_{ES}F_{GS} \rangle \text{Re}(D_{N_{ES}N_p}D_{N_{GS}N_p}^*) \\
&- 2 \langle F_{RS}F_{ES} \rangle \text{Re}(D_{N_{GS}N_p}D_{N_p N_p}^*) \Big],
\end{aligned}
\tag{17}
$$

where $D(\omega)$ is the modulation-frequency dependent determinant based on the small signal analysis' 5×5 matrix in (12). $\text{Re}(D_{XY})$ is the real part of the subdeterminant $D_{XY}(\omega)$, where the suppressed row and column of the determinant D correspond to the rate equation variables X and Y, respectively.

3. Numerical results and discussion

In this section, the response of the QD gain chip to the EC is simulated considering different parameter variations. More specifically, the analyses focus on the dynamic and noise properties assuming different values for ℓ_{ext}, ε, and α_H. The outcoupling mirror R_2 has a nominal value fixed to 10^{-4}. All other parameters used in the simulations are displayed in table 1. Results are compared with respect to the solitary laser for which $R_3 = 0$ and $R_2 = 0.32$.

3.1. Turn-on delay

The turn-on delay is evaluated at first. Figure 3 shows two main features both at 1.5 and 3.5 times the threshold current I_{th}. As the current injection is increased, the delay time is decreased, which is expected since the higher the current, the more carriers are flooded into the active material. The simulations also
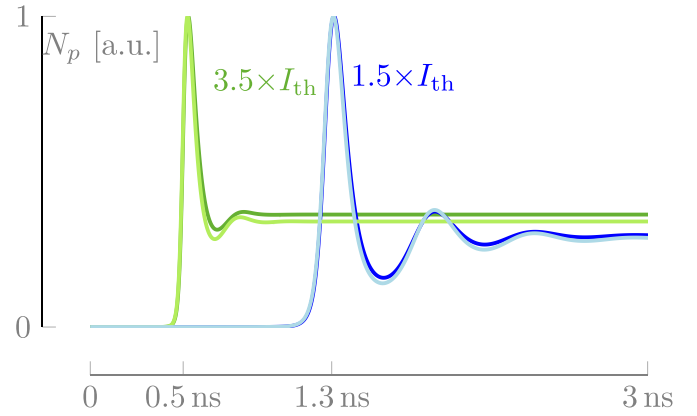

Figure 3. The turn-on delays simulated for different values at 1.5 and 3.5 times the threshold current I_{th} (blue and green, respectively) behave as expected. Resulting higher absolute output powers with EC (dark colors) are almost superimposed with respect to their solitary cases (light colors) due to normalization.

confirm that both the relaxation oscillation and the damping frequency increase with the bias current [24]. For instance, the oscillation frequency at 1.5 and $3.5 \times I_{th}$ is 2.7 GHz and 6.2 GHz, respectively.

3.2. Steady-state conditions

Figure 4(a) displays the GS carrier number with respect to the injected current. First, it is calculated at $\varepsilon = 0$ (no gain compression) for different EC lengths, i.e. 6 mm (red), 1.5 cm (orange), 3 cm (green), 6 cm (blue), and 9 cm (purple). The upper dashed curve depicts the solitary case. Simulations show two main effects: first, the GS population gets clamped at a certain injected current, where the GS lasing emission starts. Second, the presence of an EC leads to a clear reduction of the carrier induced gain. Figure 4(b) now shows the GS carrier number calculated for different gain compression values, while assuming a nominal value for the EC length of $\ell_{ext} = 6$ cm. Simulations confirm that due to gain compression, the carrier number must increase in order to counterbalance gain and loss associated to the threshold condition.

A decrease in the GS charge carrier number N_{GS} goes along with a slight reduction of the threshold current in the light-current characteristics, depicted in figure 5. For instance, the threshold is reduced from 29 mA (solitary) to 27 mA ($\ell_{ext} = 3$ cm). Let us also stress that the EC provides a very good way of increasing the photon number so does the output power. For instance, the photon number is enhanced from about 5.6×10^5 (no EC) to more than 7.7×10^5 (for $\ell_{ext} = 9$ cm) at 80 mA.

3.3. Damping

Similarly to the GS charge carrier numbers, we now look at the damping factor γ for both a varying EC length ℓ_{ext} and gain compression ε, while keeping the respective other value constant. Figure 6(a) displays the damping factor as a function of the squared relaxation oscillation frequency f_R. The damping factor scales up linearly and exhibits much higher
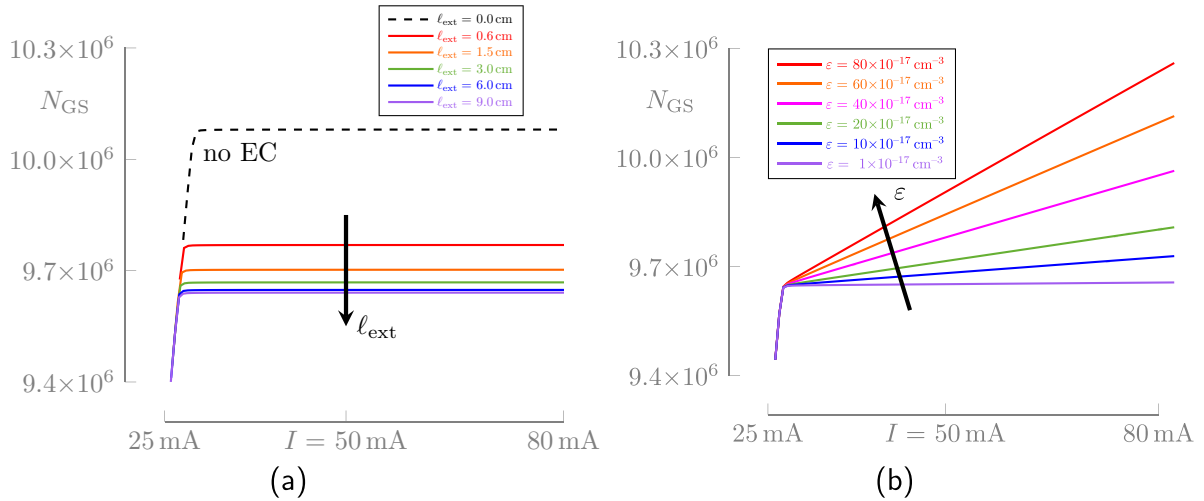
Figure 4. GS carrier number evolution with increasing current (a) for different EC lengths (in color) and the solitary case (without EC, dashed) at $\varepsilon = 0$ cm^{-3} and (b) for different gain compression factors ε at $\ell_{ext} = 6$ cm.
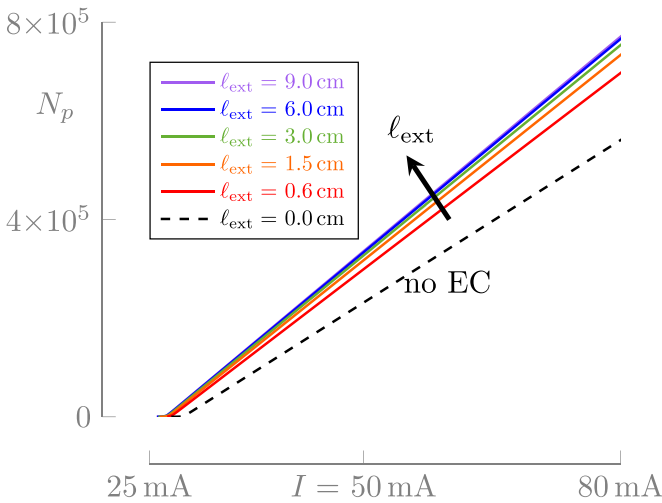

Figure 5. Light current characteristics simulated for the solitary case (dashed) and different EC lengths (in color).

values than those observed in QW lasers [24]. More specifically, the damping factor ranges from 20 GHz to more than 40 GHz depending on the bias conditions. In addition, it also depends on the EC length, hence being increased by several GHz at larger values of the EC length at 3 cm or above. This effect results from the compound cavity in which the gain chip's front-facet is AR coated, which means an increase in the photon lifetime with cavity length, leading to a larger damping. The length dependence has been part of a QW laser study [28], and although limited to internal lengths, i.e. free running diodes, we see a similar behavior for our QD EC laser case hence when the damping factor increases with the photon lifetime.

As for the influence of the nonlinear gain, simulations show that the higher the gain compression factor ε, the higher the damping factor (figure 6(b)). For instance at $f_R^2 = 20$ GHz^2, the damping factor is about 37 GHz at $\varepsilon = 10^{-17}$ cm^{-3}, whereas it goes up to about 44 GHz for $\varepsilon = 80 \times 10^{-17}$ cm^{-3}. Note that additionally with a higher gain compression factor, the

damping factor γ does not increase linearly with f_R^2 anymore, but the slope decreases with higher values of the relaxation oscillation frequency. This is because more and more GSs are occupied by charge carriers as a result of less ideal gain clamping.

3.4. Noise

The model shows a known and expected behavior for noise. Figure 7(a) confirms the working of the model through typical RIN spectra, simulated at $1.5 \times I_{th}$ (solid red curve), $2.5 \times I_{th}$ (green dashed curve), and $3.5 \times I_{th}$ (blue dotted curves) considering a threshold current of $I_{th} = 27.2$ mA and a fixed EC length of $\ell_{ext} = 6$ cm. Below the relaxation peak, a constant RIN value is predicted [4], for instance at 1 MHz, it decreases from -151.9 dB Hz^{-1} at $1.5 \times I_{th}$ to -161.9 dB Hz^{-1} at $3.5 \times I_{th}$. Above the relaxation peak, the RIN decreases strongly due to the larger damping factor for instance, at 20 GHz, from -152.8 dB Hz^{-1} at $1.5 \times I_{th}$ down to -159.6 dB Hz^{-1} at $3.5 \times I_{th}$.

Figure 7(b) illustrates the impact of the EC length in the RIN spectrum: Confirming the work on QW EC lasers by Hisham *et al* [29], no significant change is observed. The reason for this behavior is attributed to the photon lifetime τ_p that is calculated here by considering the complete cavity as travel distance. Said differently, the second mirror reflectivity R_2 is considered only as a perturbation with respect to the total cavity $\ell_{int} + \ell_{ext}$. As a result, changing the value of ℓ_{ext} is found to be less influential on the RIN.

As for the impact of the AR coating, we decided to unveil its impact on the RIN spectrum. Simulations show that no major change is unveiled on the RIN spectrum and on the damping factor (figure 7(c)), which proves that the EC QD gain chip exhibits a very good tolerance against any AR coating impairment. This is again coherent with results obtained with other models in literature, such as on a fiber grating Fabry–Perot QW EC laser [29]. In other words, there is no need to go to lower values than $R_2 = 10^{-3}$ considering that a power reflectivity of 10^{-4} is practically attainable. Thus, relatively small variations
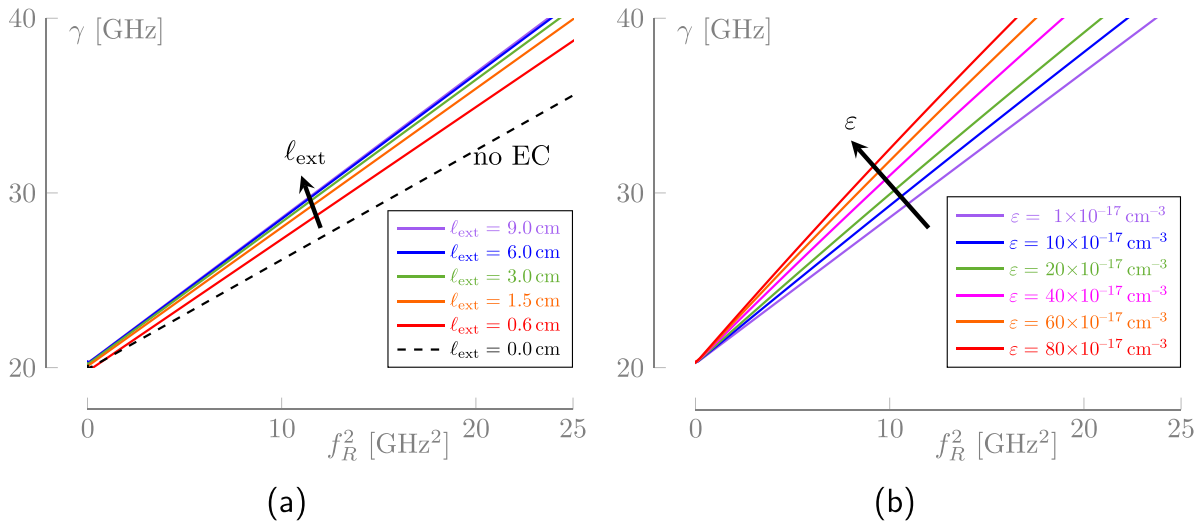
Figure 6. Damping factor γ as a function of the squared relaxation oscillation frequency f_R^2 (a) for the solitary case (without EC) compared to different EC lengths and (b) for different gain compression factors ε.
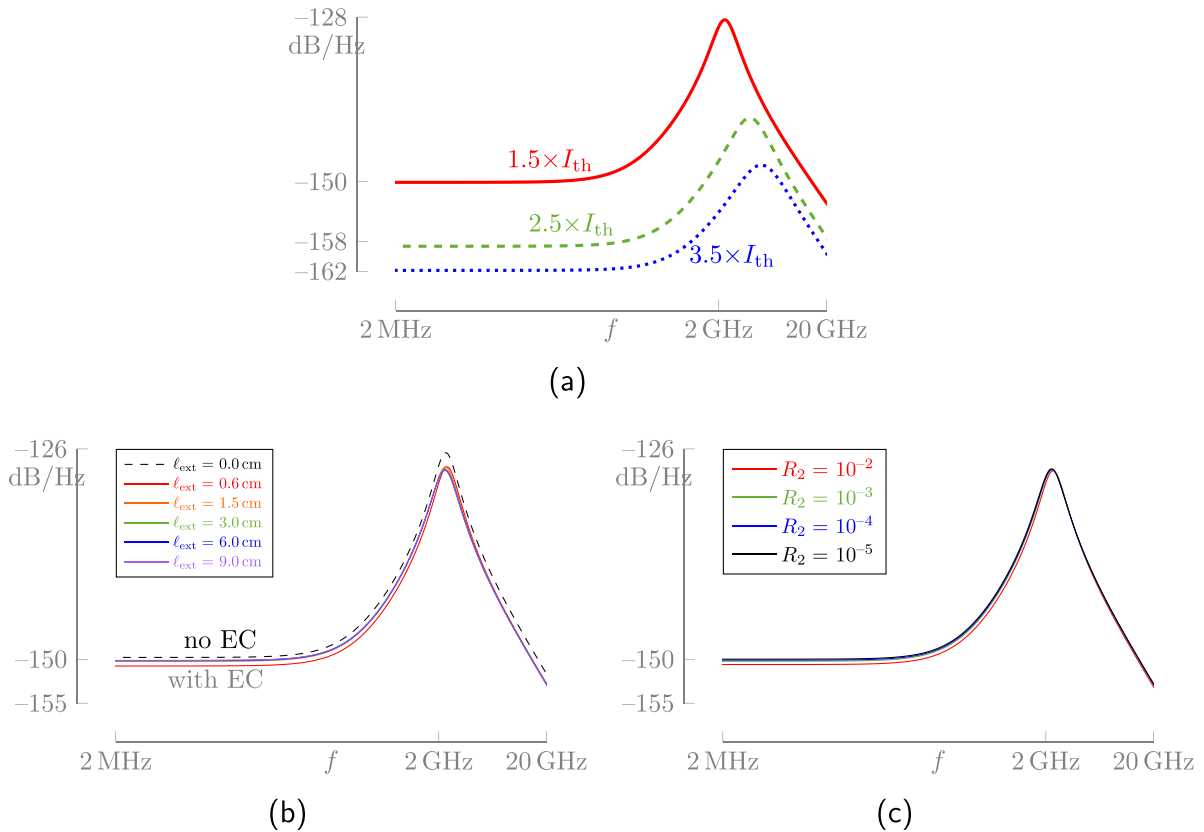

Figure 7. Simulations of the RIN (a) show the expected decrease for different normalized bias currents (at $\ell_{\text{ext}} = 6$ cm; $\alpha_H = 1$), (b) for different EC lengths show no significant impact (at $1.5 \times I_{\text{th}}$) and (c) no impact, either, for different front facet AR coating impairment assuming different power reflectivities R_2 (at $\ell_{\text{ext}} = 6$ cm; $1.5 \times I_{\text{th}}$).

in the AR coating can be allowed without altering the overall device performance.

Regarding the gain compression factor ε, figure 8 shows the impact this parameter has on the RIN and FN. Increasing the nonlinear gain coefficient from 1×10^{-17} cm^{-3} to 80×10^{-17} cm^{-3} reduces the magnitude of the peak for the FN and RIN, which is attributed to the increase of the damping factor. This

behavior has similarly been simulated before, e.g. for a QW fiber Bragg Fabry–Perot [29]. In both noise situations of this work, this reduction of the peak amplitude with the gain compression also comes with a relatively small frequency shift of the peak value. For instance for the FN, the shift ranges from about 2.7×10^5 Hz^2/Hz at $f = 2.2$ GHz to 1.2×10^5 Hz^2/Hz at $f = 1.8$ GHz; whereas for the RIN, it moves from about
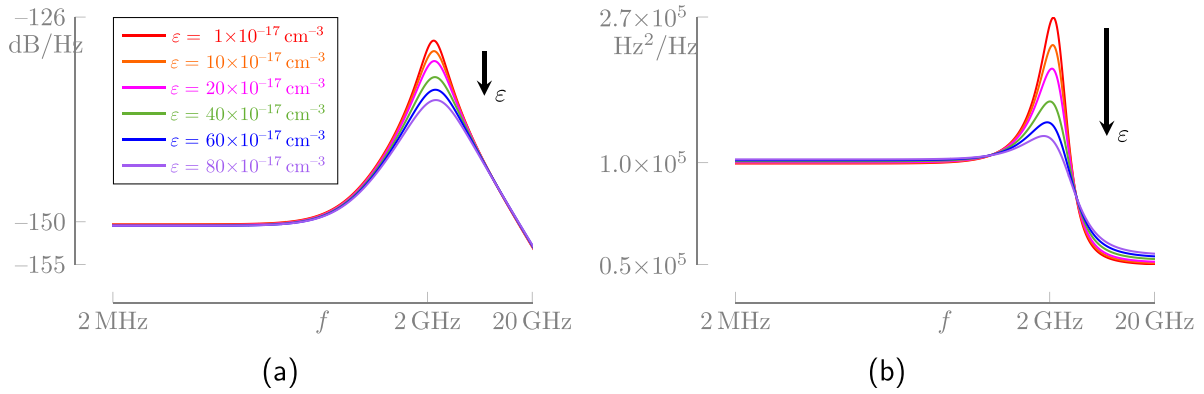
Figure 8. Simulations confirm the model's validity with respect to different gain compression factors ε at $1.5 \times I_{\text{th}}$ and $\ell_{\text{ext}} = 6$ cm of (a) the RIN and (b) the FN. The peak values in all spectra decrease with increasing ε in the indicated direction. The legend is valid for both (a) and (b).
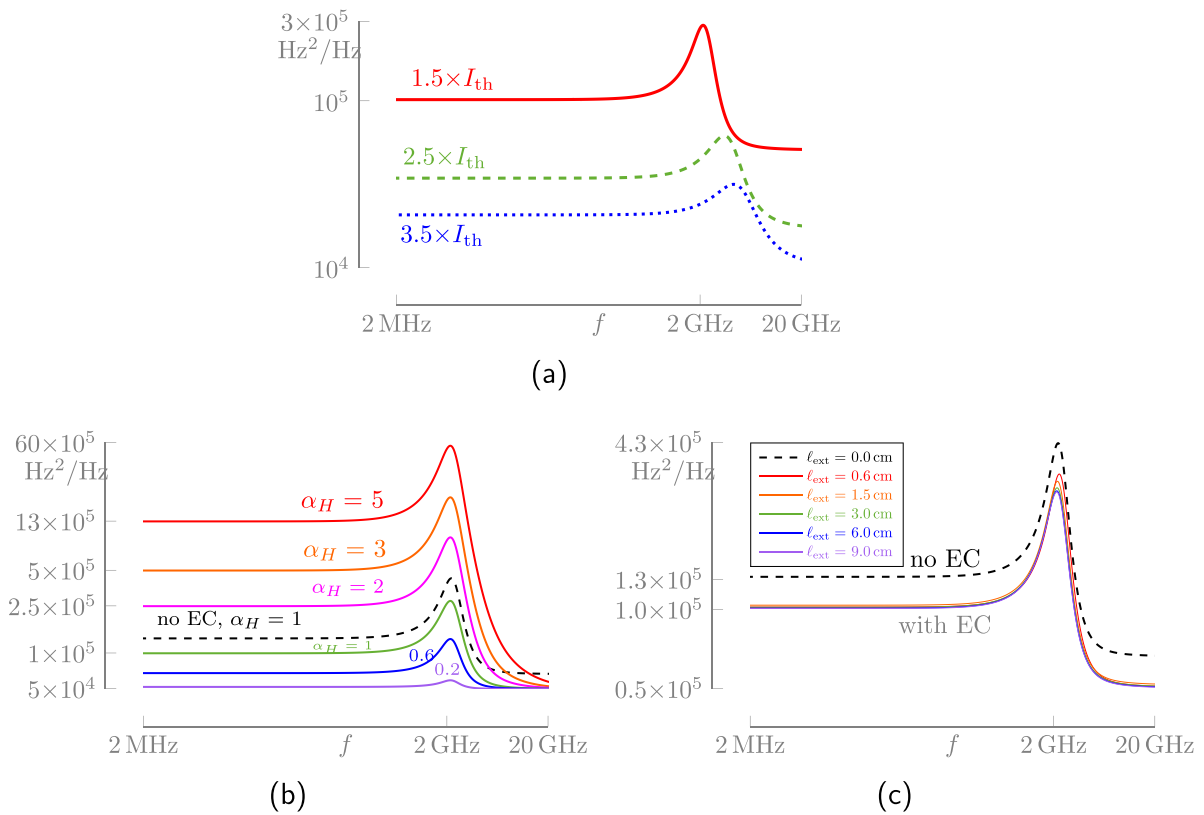

Figure 9. Simulations of the FN (a) show the expected decrease and well-known behavior for different normalized bias currents (at $\ell_{\text{ext}} = 6$ cm; $\alpha_H = 1$), (b) for different indicated values of the linewidth enhancement factor α_H (at $\ell_{\text{ext}} = 6$ cm; $1.5 \times I_{\text{th}}$) with respect to the solitary case (without EC, dashed) and (c) showing the impact for different EC lengths (at $1.5 \times I_{\text{th}}$; $\alpha_H = 1$) with respect to the solitary case (without EC, dashed).

-128.8 dB Hz^{-1} at $f = 2.3$ GHz to -135.7 dB Hz^{-1} at $f = 2.4$ GHz.

The FN is linked to the spectral linewidth through the relationship $\Delta\nu = 2\pi \text{FN}|_{f \ll f_{\text{R}}}$ [8, 30]. With the increase of injection current, the FN shows an expected and typical decreasing behavior in the simulation (figure 9(a)), confirming the model. Here, at a constant EC length $\ell_{\text{ext}} = 6$ cm and $\alpha_H = 1$, the FN is about 10×10^4 Hz^2/Hz at $1.5 \times I_{\text{th}}$ hence resulting in a spectral linewidth of about 640 kHz, which is further compressed down to FN $= 2.1 \times 10^4$ Hz^2/Hz at $3.5 \times I_{\text{th}}$ hence resulting in

$\Delta\nu \approx 130$ kHz. These values are narrower than those obtained with QW technology whereby typical solitary linewidths are around 1 MHz against less than 200 kHz for QD ones [31, 32].

The main impact of the linewidth enhancement factor α_H is displayed in the FN spectrum (figure 9(b)). Indeed, the lower the linewidth enhancement factor, the lower the FN at low frequencies, which, in turn, implies a narrower spectral linewidth. For instance, assuming $\ell_{\text{ext}} = 6$ cm at $1.5 \times I_{\text{th}}$, the FN is about 10×10^4 Hz^2/Hz at $\alpha_H = 1$ hence resulting in a spectral linewidth of about 640 kHz, which is further

decreased down to 5.2×10^4 Hz^2/Hz at $\alpha_H = 0.2$ hence resulting in $\Delta\nu \approx 325$ kHz.

Lastly, figure 9(c) illustrates a 'binary' behavior, i.e. that the FN is only sensitive to the existence of an EC, and the exact length of the EC is less important. Thus, considering EC lengths of a few centimeters, the FN spectrum is reduced compared to its solitary laser (upper dashed curve), i.e. $\ell_{ext} = 0$ cm and $R_2 = 0.32$. This noise reduction is not observed on the RIN counterpart (figure 7(b)). At the same current of $1.5 \times I_{th}$, the free-running configuration leads to a FN of 1.33×10^5 Hz^2/Hz hence resulting in a broader spectral linewidth of about 840 kHz and thus higher than with any of the simulated EC lengths.

4. Conclusions

Owing to a rate equation model successfully applied to an EC QD gain chip-based laser with strong optical feedback, simulation unveils the importance of the design of the EC on the dynamic and noise characteristics with respect to the material and device parameters such as gain compression and linewidth enhancement factor. Another key parameter is the EC length and thus the photon lifetime, whose variations barely evoke any influence around the simulated lengths of a few centimeters (as opposed to the solitary case). Non-critical as well is the simulated small reflectivity of the gain chip outcoupling-mirror. An EC in itself decreases thus the threshold current, the linewidth, but not the RIN. It also increases the output power and the damping. Additionally, an increase in the gain compression factor decreases the peak magnitude of the noise figures. Finally, an increase in the bias current or a decrease in the linewidth enhancement factor results in a lower frequency noise. Therefore, we believe that these numerical investigations give new insights in terms of design guidelines for the realization of future QD gain chip-based EC lasers.

Acknowledgment

ORCID iDs

Jannik F Ehlert ⬤ https://orcid.org/0000-0003-1713-5342
Frédéric Grillot ⬤ https://orcid.org/0000-0001-8236-098X

References

[1] Li S G, Gong Q, Cao C F, Wang X Z, Yan J Y, Wang Y and Wang H L 2014 *Opt. Quantum Electron.* **46** 623–40

[2] Mroziewicz B 2008 *Opto-Electron. Rev.* **16** 347

[3] Shoshan I, Danon N N and Oppenheim U P 1977 *J. Appl. Phys.* **48** 4495–7

[4] Duan J, Wang X, Zhou Y, Wanga C and Grillot F 2018 *IEEE J. Quantum Electron.* **54** 1–7

[5] Deppe D G, Shavritranuruk K, Ozgur G, Chen H and Freisem S 2009 *Electron. Lett.* **45** 54–6

[6] Liu G T, Stintz A, Li H, Malloy K J and Lester L F 1999 *Electron. Lett.* **35** 1163–5

[7] Huang H, Duan J, Dong B, Norman J, Jung D, Bowers J E and Grillot F 2020 *APL Photon.* **5** 016103

[8] Wang C, Zhuang J P, Grillot F and Chan S C 2016 *Opt. Express* **24** 29872–81

[9] Becker A *et al* 2016 *Proc. SPIE* **9767** 97670Q

[10] Kita T, Tang R and Yamada H 2016 *IEEE J. Sel. Top. Quantum Electron.* **22** 23–34

[11] Malik A, Guo J, Tran M A, Tran M A, Kurczveil G, Liang D and Bowers J E 2020 *Photon. Res.* **8** 1551–7

[12] Arakawa Y 2016 Quantum dot lasers for silicon photonics *2016 21st OptoElectronics and Conf. (OECC) Held Jointly With 2016 Int. Conf. on Photonics in Switching (PS)* pp 1–2

[13] Chen S *et al* 2016 *Nat. Photon.* **10** 307–11

[14] Nevsky A Y *et al* 2008 *Appl. Phys.* B **92** 501–7

[15] Tkach R and Chraplyvy A 1986 *J. Lightwave Technol.* **4** 1655–61

[16] Coldren L A, Corzine S W and Mašanović M L 2012 Dynamic effects *Diode Lasers and Photonic Integrated Circuits* 2nd edn (Hoboken, New Jersey: Wiley-Blackwell) pp 247–333

[17] Lenstra D, Verbeek B and Boef A D 1985 *IEEE J. Quantum Electron.* **21** 674–9

[18] Ye C 2004 *Tunable External Cavity Diode Lasers* (Singapore: World Scientific)

[19] Even J, Wang C and Grillot F 2016 From basic physical properties of inas/inp quantum dots to state-of-the-art lasers for 1.55 μm optical communications *Semiconductor Nanocrystals and Metal Nanoparticles* (Boca Raton, FL: CRC Press) pp 95–125

[20] Veselinov K, Grillot F, Cornet C, Even J, Bekiarski A, Gioannini M and Loualiche S 2007 *IEEE J. Quantum Electron.* **43** 810–16

[21] Grillot F, Wang C, Naderi N A and Even J 2013 *IEEE J. Sel. Top. Quantum Electron.* **19** 1900812

[22] Lang R and Kobayashi K 1980 *IEEE J. Quantum Electron.* **16** 347–55

[23] Columbo L, Bovington J, Romero-Garcia S, Siriani D F and Gioannini M 2020 *IEEE J. Sel. Top. Quantum Electron.* **26** 1–10

[24] Wang C, Grillot F and Even J 2012 *IEEE J. Quantum Electron.* **48** 1144–50

[25] MATLAB 2014 *8.4.0.150421 (R2014b)* (Natick, MA: The MathWorks Inc.)

[26] Helms J and Petermann K 1991 *J. Lightwave Technol.* **9** 468–76

[27] Gensty T and Elsäßer W 2005 *Opt. Commun.* **256** 171–83

[28] Tatham M C, Lealman I F, Seltzer C P, Westbrook L D and Cooper D M 1992 *IEEE J. Quantum Electron.* **28** 408–14

[29] Hisham H K, Abas A F, Mahdiraji G A, Mahdi M A and Noor A S M 2012 *IEEE J. Quantum Electron.* **48** 375–83

[30] Ohtsubo J 2012 *Semiconductor Lasers* (Berlin: Springer)

[31] Duan J, Huang H, Lu Z G, Poole P J, Wang C and Grillot F 2018 *Appl. Phys. Lett.* **112** 121102

[32] Septon T *et al* 2019 *Optica* **6** 1071–7